micromachines

Article

$Ti_3C_2T_x$ MXene-Polymeric Strain Sensor with Huge Gauge Factor for Body Movement Detection

Wei Xian Rebecca Leong [1,2], Adel Mohammed Al-Dhahebi [2,3], Mohamad Radzi Ahmad [2,4] and Mohamed Shuaib Mohamed Saheed [2,3,*]

[1] Department of Fundamental and Applied Sciences, Universiti Teknologi PETRONAS, Seri Iskandar 32610, Perak, Malaysia
[2] Centre of Innovative Nanostructure & Nanodevices (COINN), Universiti Teknologi PETRONAS, Seri Iskandar 32610, Perak, Malaysia
[3] Department of Mechanical Engineering, Universiti Teknologi PETRONAS, Seri Iskandar 32610, Perak, Malaysia
[4] Department of Electrical & Electronics Engineering, Universiti Teknologi PETRONAS, Seri Iskandar 32610, Perak, Malaysia
* Correspondence: shuaib.saheed@utp.edu.my; Tel.: +60-53687653

Abstract: In this work, a composite strain sensor is fabricated by synthesizing MXene and deposition of polypyrrole on top of the flexible electrospun PVDF nanofibers. The fabricated sensor exhibits a conductive network constructed with MXene and polypyrrole of microcracks network structure, demonstrating its strain sensing properties. The presence of these microcracks serves as mechanical weak points, which leads to sensitivity enhancement, while the electrospun fiber substrate act as a cushion for strain loading under large deformations. The as-prepared MXene@Polypyrrole PVDF sensor has a gauge factor range of 78–355 with a sensing range between 0–100%. Besides strain deformations, the sensor can operate in torsional deformation and human motion, indicating the sensor's potential as a wearable health monitoring device.

Keywords: $Ti_3C_2T_x$-MXene; polypyrrole; strain sensing; torsion

check for updates

Citation: Leong, W.X.R.; Al-Dhahebi, A.M.; Ahmad, M.R.; Saheed, M.S.M. $Ti_3C_2T_x$ MXene-Polymeric Strain Sensor with Huge Gauge Factor for Body Movement Detection. *Micromachines* **2022**, *13*, 1302. https://doi.org/10.3390/mi13081302

Academic Editors: Hong Ding, Jin Xie and Zebing Mao

Received: 12 July 2022
Accepted: 6 August 2022
Published: 12 August 2022

1. Introduction

MXene, a new class of 2D material, has been researched broadly recently. This material class comprises layers of transition metal/carbides, nitrides, or carbonitrides [1]. MXene is stripped from the ternary ceramic structure carbide and nitrides with the formula $M_{n+1}AX_n$, n = 1,2, or 3, where M is the transition metal (Ti, V, Cr, Mo, Nb, etc.), A is mainly group 13 and 14 elements (Si, Al, Ge or Sn) and X is carbon, nitrogen or both [2–4]. The combination of ceramic and metallic behaviors makes the MAX phase distinctive. MAX phase exhibits high hardness, low density, and resistance to corrosion. Besides, its high thermal and electrical conductivity properties are near to metallic materials [5]. Among the different classes of MXene, Ti_3 C_2 T_x is highly investigated. A high selectivity etching agent is crucial to etch the Al atom layer from the Ti_3AlC_2 accurately. MXene is synthesized from its parental MAX precursor phase using the topochemical selective etching process. The principle of this method involves the use of chemical etchant (hydrofluoric acid (HF) or hydrochloric acid/lithium fluoride (HCL/LiF)) to etch or substitute (delaminate) the strong M-A bonds (in the MAX phase) with weaker hydroxyl (OH), oxygen (O), fluorine bonds. The resultant materials typically possess stoichiometry structure of $M_{n+1}X_nT_x$ layers (called MXene) in which the T_x describes the surface functional groups (OH, O, and F) [1]. These surface terminations render MXene hydrophilic functionality and processability compared to other 2D nanomaterials such as graphene and transition-metal dichalcogenides (TMDs). As a result, MXene based materials have recently captivated the interests of scientists and engineers across various disciplines not only in biomedical applications but also in wearable, soft electronics and energy storage devices [5].

Strain sensors or conventionally known as strain gauge have been in the market for decades. The basic concept of a strain sensor is it transduces mechanical deformations into electrical signals. Flexible and stretchable strain sensor still focus on piezoresistive and capacitive type due to their simple read-out system and high flexibility and stretchability. Common intrinsic stretchability of strain sensor is incorporated with conductive materials such as carbon black, graphene, carbon nanotubes (CNTs) and metal nanostructures (e.g., AgNWs) into stretchable elastomeric matrix. Stretchable conductors with huge difference in electrical properties during deformation are commonly utilized in stretchable devices. However, there are several drawbacks associated with these nanostructured conductive materials such as low electrical conductivity (carbon black), irreversible cracks after deformation (graphene), poor purity causing large resistance (CNT) and relatively high cost fabrication process (AgNWs) [5].

Recently, MXene-based strain sensors performance outperformed previously reported hydrogel [6] and MoS_2 [7]. They exhibit characteristics of high sensitivity, fast response, good stability, and excellent conformability. Due to MXene hydrophilic behavior has good interaction with polymeric matrixes, it is favorable in synthesis of hybrid composite materials. This composite can be processed through simple and low-cost methods into films, fibers and 3D structures attributed to easy fabrication methods such as electrospraying. Several polymer matrixes were reported, including polyvinyl alcohol (PVA) [8–10], poly(vinylidene fluoride), polyacrylamide (PAM) [11], polyethylene [12], polyurethane (PU) [13], polyfluorenes [14] and polydiallyldimethylammonium chloride (PDDA) [8] which were utilized as a base substrate for flexibility of the strain sensor. However, MXene incorporation affects the structure and crystallization rate of the polymer matrix which influences the overall performance of the device [12]. Among various conducting polymers, polypyrrole (PPy) is one of the most successful electrode materials due to its easy synthesis, low cost, and high conductivity [15]. In previous studies, conductive PPy/PU composites fabricated strain sensors with high stretchability but had relatively low sensitivity for a strain sensing application [16]. Recently, another group of researchers produced MXene/PVDF composite to demonstrate the excellent contribution of MXene to electrical performance [17]. To the best of our knowledge, there are no reports on incorporating MXene nanosheets with PPy on PVDF nanofiber in the application of strain sensing and human motion monitoring. Despite the excellent properties of polymer and MXene composite, there is still limited detailed study that discussed the changes in conductivity and structures of polymeric composites with MXene, crucial in utilizing for real-time applications such as in healthcare.

Herein, we report a process using $Ti_3C_2T_x$ MXene and polypyrrole as conductive material and electrospun polyvinylidene fluoride (PVDF) as the flexible substrate. The synthesized MXene powder was mixed in stoichiometric ratio with pyrrole monomer, then deposited on the electrospun PVDF substrate. The fabricated conductive flexible substrate is processed into sensor packaging for electromechanical characterization.

2. Materials and Methods

2.1. Preparation

2.1.1. Synthesis of MXene

The MXene powder $Ti_3C_2T_x$ was prepared using the chemical liquid etching method adopted from Alhabeb et al. [18]. The precursor material Ti_3AlC_2 (99 wt%, Luoyang Tongrun Info Technology Co., Ltd., Luoyang, China) was etched by the Al layer via 9 M HCl (37 wt%, Sigma–Aldrich, St. Louis, MO, USA) and 12M LiF (99 wt%, Sigma–Aldrich, St. Louis, USA). During the acid etching process, Ti_3AlC_2 powder was introduced into the acid mixture at a ratio of 1 g:10 mL under continuous stirring for 24 h at room temperature. The resulting mixture was washed with distilled water and centrifuged at 7500 rpm for 5 min until the pH was above 6. The precipitates were then collected by vacuum filtration through PVDF membrane and dried in a vacuum oven at 80 °C for 6 h. The dried residues are collected from the PVDF membrane for further characterization.

2.1.2. Electrospun PVDF Fabrication

Electrospinning is a versatile and viable technology capable of manufacturing various nanofibrous assemblies from a variety of raw materials (polymers, metals, ceramics, etc.) with specialized features such as large surface area, interconnected and porous structures, easy functionalization and surface modification, and mechanical robustness [19]. The unique features of electrospun nanofibers make them appealing for the design of high-performance wearable and strain sensors, biomedical devices, energy storage and filters [20,21]. Electrospinning was used to fabricate electrospun PVDF nanofibers and discussed in great detail in our previous publications [22,23]. Briefly, electrospun PVDF solution was prepared by dissolving 20 wt.% in acetone/dimethylformamide (DMF) (2:3 v/v) and magnetically stirred at 60 °C for 5 h to dissolve the PVDF followed by stirring overnight at room temperature to obtain homogenous solution. The solution was loaded into a 10 mL plastic syringe with stainless steel needle (21 G) and used for electrospinning (ES: Model TL-Pro-BM) under spinning conditions of 2 mL/h flow rate, 15 cm as fiber receiving distance, and 18 kV electrical applied voltage. The electrospinning process was conducted at room temperature and with less than 30% relative humidity. The ejected nanofibers were collected using a grounded metallic collector that was covered with aluminum foil and revolving at 400 rpm. The electrospun nanofibers were dried in a drying oven at 60 °C for 12 h to remove the residual solvents. The electrospun PVDF nanofibers were then used for the preparation of the strain sensor as illustrated in the subsequent section.

2.1.3. Sensor Fabrication

First, $FeCl_3$ solution with different concentrations was prepared ranged from 0.1 M to 0.5 M. Electrospun PVDF strips are cut into the desired length ($5 \times 1\ cm^2$) [24] and soak in $FeCl_3$ solution of different concentrations for 2 h. Pyrrole monomer and anhydrous ethanol were mixed in 1:1 ratio as pyrrole solution. 5 wt% of MXene in pyrrole solution was prepared and ultrasonicated for 30 min. The electrospun PVDF strip was then laid flat on Teflon plates with 5 wt% MXene-PPy solution drop coated on top of the PVDF strip. The process of reaction was allowed for 2 h and the PVDF strip was rinsed with DI water and ethanol. The conductive PVDF strip was then sandwiched between flexible VHB tape (4910F, 3M) and attached with copper tape at both ends of the conductive PVDF strip as indicated in Figure 1. Different sensing films denoted as $Ti_3C_2T_x/PPy_{0.1}/PVDF$, $Ti_3C_2T_x/PPy_{0.2}/PVDF$, $Ti_3C_2T_x/PPy_{0.3}/PVDF$, $Ti_3C_2T_x/PPy_{0.4}/PVDF$ and $Ti_3C_2T_x/PPy_{0.5}/PVDF$ are designed and fabricated, respectively. The subscript numbers represent the concentration of the $FeCl_3$ used.

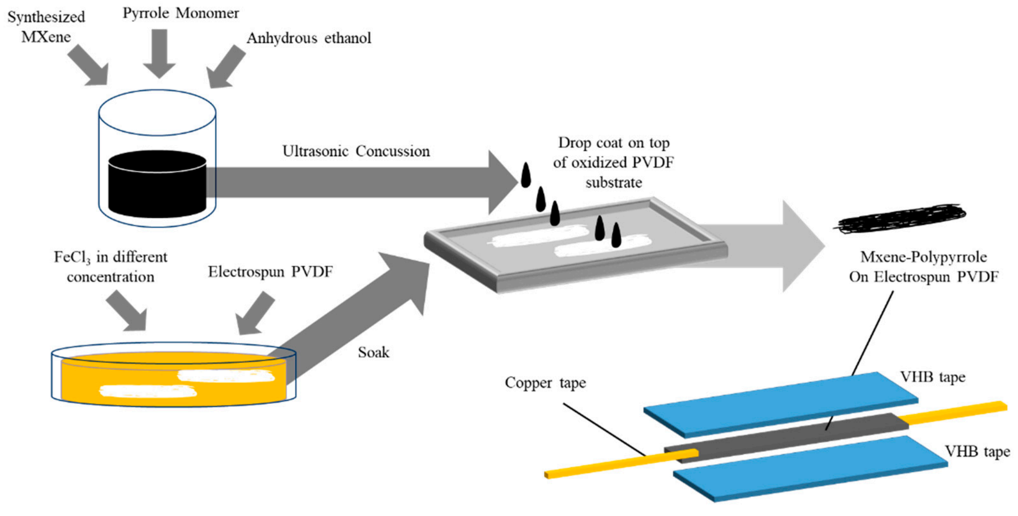

Figure 1. Schematic diagram of fabrication process of Mxene@Polypyrrole electrospun PVDF sensor.

2.2. Characterization

Characterization tools used were Field Emission Scanning Electron Microscope (FE-SEM, Supra 55VP, ZEISS, Jena, Germany), Transmission Electron Microscopy (TEM, HT7830, Hitachi, Tokyo, Japan), and X-ray Photoelectron Spectroscopy (XPS, K-Alpha, Thermo, Waltham, MA, USA). The X-ray diffraction spectrum of the samples was obtained on a powder X-ray diffractometer (Xpert3 Powder, Panalytical, Malvern, UK) using Cu Kα ($\lambda = 1.5418$) radiation as the light source. The 2θ angle was investigated for 5–80°. The FTIR spectra were recorded on Fourier-transform infrared spectroscopy (FTIR, Frontier, Perkin Elmer, Waltham, MA, USA). The electromechanical characterization of the strain sensors was measured with a static in-house build sensor holder and a digital multimeter (31944A, Keysight, Santa Rosa, CA, USA). All characterizations are performed in room temperature.

3. Material Characterization

A schematic illustration of the PVDF/$Ti_3C_2T_x$ MXene@Polypyrrole strain sensor fabrication procedure is illustrated in Figure 1. First, a mixed solution of synthesized MXene ($Ti_3C_2T_x$) nanosheets pyrrole monomer was prepared through an ultrasonic concussion to produce the conductive filler solution. The flexible substrate, electrospun PVDF nanofiber was prepared by soaking in initiator solution and conductive filler solution was coated on top of the flexible substrate producing a conductive flexible electrode. The conductive substrate was then packaged into a functional strain sensor.

Figure 2a shows the FESEM image of MXene nanosheets, confirming the etching of Al and delamination of MXene layers. Additionally, in Figure 2b the TEM image of MXene nanosheets indicates MXene sheets are well exfoliated. The most intense XRD peak (002) at 9° confirmed the proper synthesis of MXene as shown in Figure 2e. The surface functionalization of MXene was analyzed with XPS, shown in Figure 2d. The XPS spectrum exhibit the presence of F, O, Ti, and C elements with the notable absence of the metallic Al. The binding energies of the core peak position of F, O, Ti, and C elements are 684.7, 532.4, 455.8, and 284.9 eV, respectively. The presence of O and F indicates the surface of MXene film is functionalized by –O, –OH, and –F groups which is consistent with previous reports [17]. Besides that, no significant peak observed between 70–80 eV represents the Al 2p peak of MAX phase, further confirming the successful synthesis of MXene.

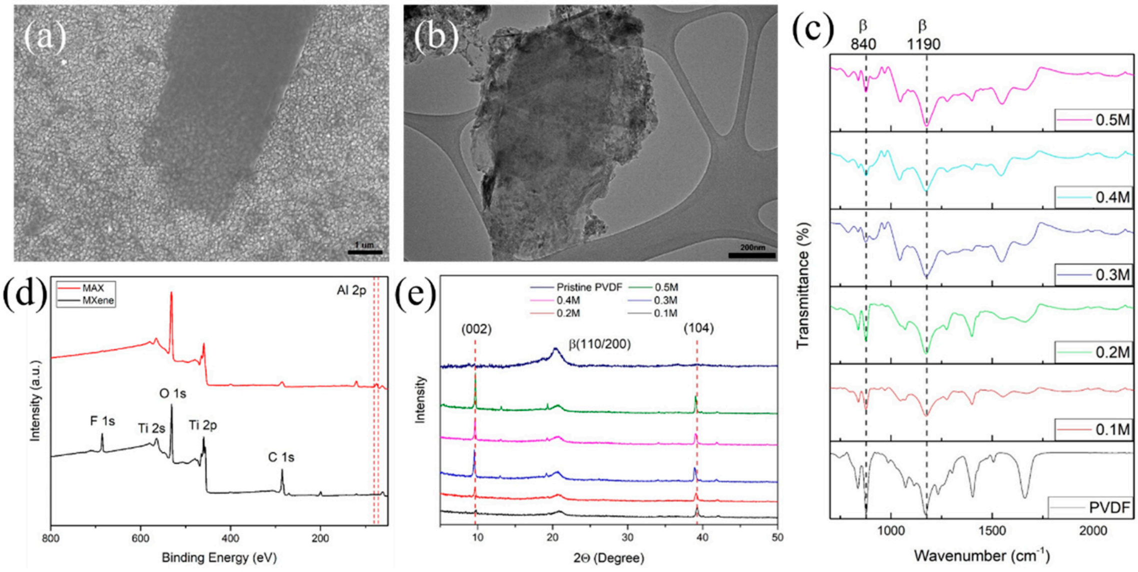

Figure 2. (**a**) FESEM images of $Ti_3C_2T_x$ nanosheets (**b**)TEM images of $Ti_3C_2T_x$ nanosheets (**c**) FTIR spectrum of various $FeCl_3$ concentration (**d**) XPS spectrum of MAX phase and $Ti_3C_2T_x$ nanosheets (**e**) XRD spectrum of electrospun PVDF and various $FeCl_3$ concentration.

The PVDF sheets employed in this study is an electrospun PVDF consisting of chemical structures of β-phase of the PVDF [22,23]. The spinning process consists of viscous PVDF precursor solution melt in applied electric field, causing uniaxial stretching due to the repulsion of the electrostatic force between surface charges. This develops the transition of α-phase crystallization into the β-phase crystallization of electrospun PVDF nanofiber [25]. The flexible electrospun PVDF nanofiber substrate will be decorated with MXene and polypyrrole, making the overall structure conductive. Polar functional groups such as –O, –OH, and –F groups are formed on the surface of MXene after chemical etching, leading to oxidation and decreasing the conductivity of MXene. Therefore, to improve the long-term stability of MXene is through modification by integrating PPy. The polymerization of PPy includes an initiator, $FeCl_3$. The polymerization of pyrrole monomers can be controlled to form PPy on the surface of MXene and PVDF substrate. The deposition of PPy not only facilitates the assembly of MXene onto PVDF substrate but also improves the non-conductive electrospun PVDF nanofiber by varying the amount of initiator. The PVDF substrate act as a support network for the formation of polypyrrole along with $Ti_3C_2T_x$ MXene nanosheets. The synergy of the composition harmoniously modifies the fibre with electrical properties.

The surface morphology of the fabricated flexible PVDF substrate after the deposition of conductive filler was analyzed by FESEM, XRD, and FTIR analysis. Figure 2e shows the XRD analysis of PVDF substrate with different concentrations of the precursor solution. The strong prominent peak (002) and (104) planes at 9.6° and 38.7°, respectively, for all the fabricated samples obtained from the MXene nanosheets. As filler concentration increase, the β-characteristic (110/200 planes) become wider. The FTIR spectra are illustrated in Figure 2c. The intensity corresponding to the absorption bands at 840 and 1190 cm^{-1} of the β-crystal plane is reduced after increasing the concentrations of precursor solution in the PVDF, which also follows the observation in the XRD pattern. Figure 3a shows the cross-sectional FESEM image of $Ti_3C_2T_x$/PPy coated electrospun PVDF, which clearly represents the deposited conductive layer is firmly attached without peeling or revealing the surface of the PVDF layer. Moreover, the uniform element C, O, Ti, and F distribution from EDX mapping in Figure 3b further substantiate the uniform integration of PPy chains and MXene nanosheets.

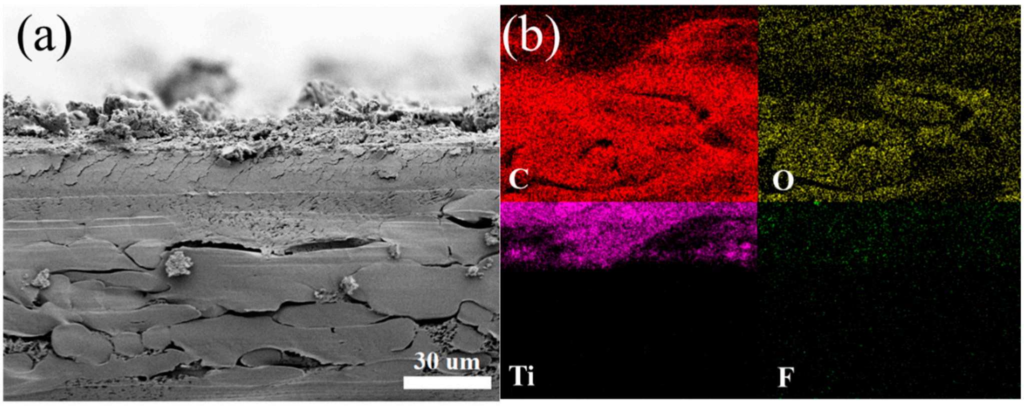

Figure 3. (**a**) Cross-sectional FESEM images of $Ti_3C_2T_x$/PPy coated electrospun PVDF (**b**) EDS elemental mapping images of C, O, Ti, and F for the $Ti_3C_2T_x$/PPy coated electrospun PVDF.

4. Working Mechanisms

The working mechanisms of the sensor were investigated by the morphological evolution of $Ti_3C_2T_x$/PPy/PVDF under different applied tensile strains. Figure 4a demonstrates the schematic diagram of the initial stage till maximum strain is applied on the fabricated sensor. Figure 4b is the chemical structure and the scheme illustrating the chemical bond interactions between MXene, PPy and electrospun PVDF. With the introduction of PPy, strong bonds such as hydrogen bonding exist between the PPy chains, MXene nanosheets and

PVDF nanofiber. Besides hydrogen bonding, H or F atoms (present in PVDF polymer and MXene surface functionalized group) has electrostatic attractions which provides stability to the layer structure [17]. As shown in Figure 4c, the $Ti_3C_2T_x$/PPy/PVDF under a relaxed state exhibits randomly distributed MXene nanosheets on PVDF fibers, interconnected as a network structure.

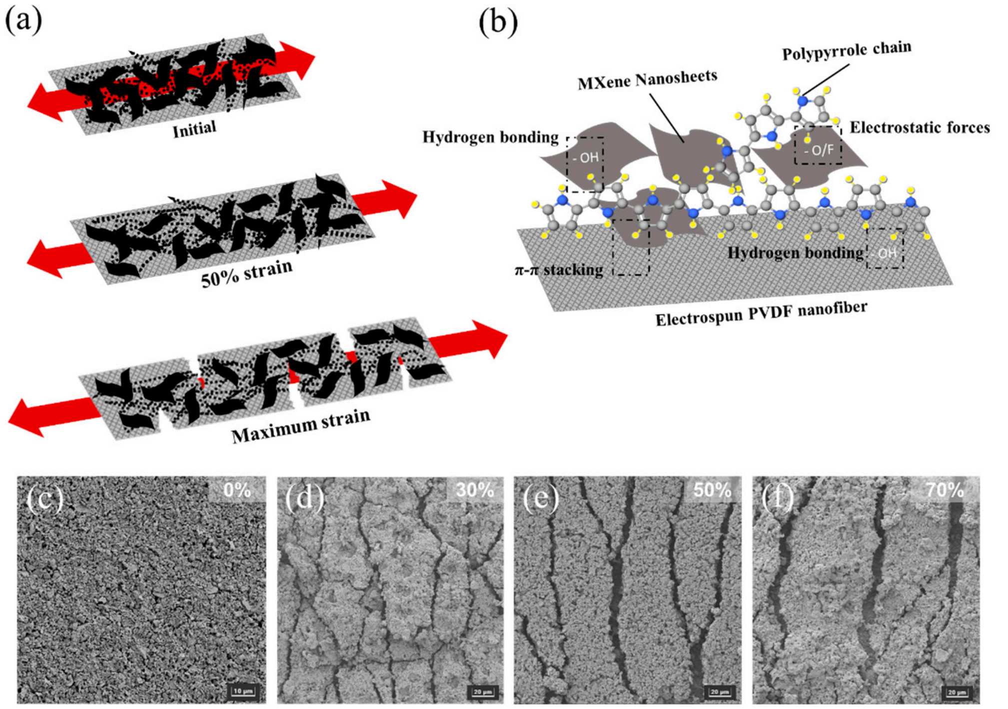

Figure 4. (**a**) Proposed sensing mechanism of Mxene/PPy electrospun PVDF sensor. (**b**) Illustration of chemical structure and interaction of MXene/PPy blending into the PVDF matrix to form an H-bonding. Morphology of the $Ti_3C_2T_x/PPy_{0.4}$/PVDF under tensile strain of (**c**) 0% (**d**) 30% (**e**) 50% (**f**) 70%.

Before stretching, the conductive layer surface is smooth with an integrated conductive network. Tensile strain was calculated as $(L - L_0)/L_0$, where L and L_0 are deformed and original lengths, respectively. Figure 4d–f shows the morphology of the $Ti_3C_2T_x/PPy_{0.4}$/PVDF under different elongation of strain. During tensile strain loading, the film is stretched along with the conductive network. At small and medium strains, the MXene and polypyrrole layer begins to break and slide from the PVDF fiber. Several microcracks appear on the surface of the MXene nanosheets layer indicating damage to the conductive network. There is still part of the polypyrrole network distributed randomly within the layer acting as bridges to connect the MXene nanosheets. With increasing tensile strain, the gaps between microcracks on the surface of MXene coating become wider. The microcracks are the mechanically weak point of the conductive network. The increase in microcracks and the propagation of cracks formation contributed to the variation of resistance across the conductive network. Eventually, the microcracks further widen during tensile strain, and the conductive network is destroyed. As a result, the electrical resistance of the conductive film increased sharply, similar to previously reported results [26–28] as shown in Table 1. The sensitivity of the sensor is developed from both polypyrrole network and MXene nanosheets in the conductive network layer. The network structure of PVDF fiber thus provides a buffer for strain loading for large deformation, thus preserving the conductive network layer from peeling or disruption. After a repeated stretch-release cycle, the conductive MXene layer is still intact with the PVDF fiber substrate which can be attributed to good interfacial stability between electrospun PVDF fiber and the MXene sheets [29]. The stable interface may be due to the strong H-bonding interaction of the MXene surface functional group with PVDF fiber [30].

Table 1. Comparison of different material fabricated strain sensors.

Materials & Structure	Gauge Factor	Sensing Range (%)	Ref.
Conventional metal foil	2	0–5	[31]
MXene/polyimide film	46–180.1	0–2.13	[32]
MXene/air-laid paper	1–2.58	10–90	
Composite yarn doped PPy	51.2	0–40	[33]
AgNW–Ecoflex	0.7	0–50	[34]
Polypyrrole (PPy)/PU	1.3	0–40	[16]
Graphene/PDMS	151	0–5	[35]
Carbon Black/PDMS	12	0–30	[36]
MXene/PPy/Electrospun PVDF	44.31–355.32	0–100	This work

5. Electromechanical Characterization and Sensing Demonstrations

The performance of the strain sensor based on $Ti_3C_2T_x$/Polypyrrole electrospun PVDF was investigated. The fabricated $Ti_3C_2T_x$/PPy/PVDF substrate for strain sensing can be tuned by adjusting the concentration of $FeCl_3$, which is the initiator used to deposit polypyrrole and MXene nanosheets. Figure 5a shows the I–V curves are straight and smooth lines. As the concentration of $FeCl_3$ increase, the resistance of the $Ti_3C_2T_x$/PPy/PVDF substrate reduce. When the concentration of $FeCl_3$ reaches 0.5M, the resistance increases. This may be due to the breakage of $Ti_3C_2T_x$ nanosheets and polypyrrole strain. Thick deposition layers of conductive filler may result in peeling the conductive filler layer from the nanofiber structures.

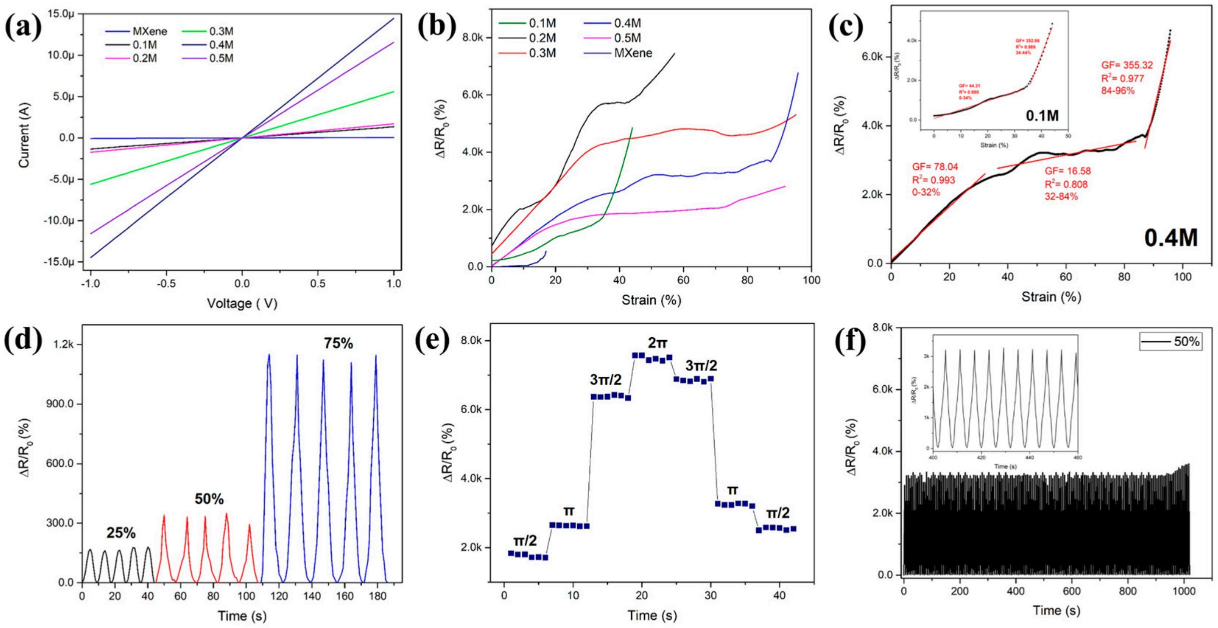

Figure 5. Electromechanical properties of the $Ti_3C_2T_x$/PPy coated electrospun PVDF strain sensor. (**a**) Comparison of the variation of resistance change under quasi-static test for various $FeCl_3$ concentrations used to fabricate the sensor. (**b**) The relative resistance changes of various concentration of $FeCl_3$ fabricated sensor. (**c**) The relative resistance changes of 0.4M $FeCl_3$ fabricated sensor (**d**) Relative resistance change of the sensor under stretch–release cycles at maximum strain of 25%, 50%, and 75%, respectively. (**e**) Torsion performance of the sensor with relative resistance changes under different torsion degrees. (**f**) Stability test under the strain of 50% for 1000 s.

Figure 5b shows the relative resistance variation-strain curve ($\Delta R/R_0$-ε) of the $Ti_3C_2T_x$/PPy/PVDF. Generally, the relative resistance ($\Delta R/R_0$) where ΔR represents (R-R_0), R and R_0 indicate resistance under different strain and initial resistance, respectively. ε represents the strain. This gauge factor (GF) was used to evaluate the sensitivity of the strain sensor represented by the slope of the curve $\Delta R/R_0$-ε. From Figure 5c insets, the strain sensor based on $Ti_3C_2T_x/PPy_{0.1}/PVDF$ was divided into two stages. During the strain range of 0–34%, the GF was quantified as 44.31 while the GF increased in the range of 34–44% to 352.86. The sensitivity of the sensor increases with low and smaller strain range. This could be due to the disconnection of microcrack junctions during tensile strain. When strain range increases, more microcracks appear, increasing crack-gap and crack density which can be identified with the distinct increase of GF and rapid decrease in electrical conductance. Therefore, the $Ti_3C_2T_x$/PPy/PVDF composite-based strain sensor exceeds the performance of a conventional metal foil-based sensor with GF $\approx$ 2, strain range of 5% [31]. Table 1 shows the GF of reported sensors for comparison. As the concentration of $FeCl_3$ increases, more deposition and compact network of the conductive fiber network. Thus, $Ti_3C_2T_x/PPy_{0.4}/PVDF$ shows a higher GF of 78.04 with a range of 0–32%, shown in Figure 5c. At a higher strain range of 84–96%, the sensor exhibited a GF of 355.32. Figure 5d shows the frequency response at strain ranges of 25%, 50%, and 75%. The corresponding response and recovery of each measured signal share a similar shape and height, indicating the sensor has a stable response to the applied cyclic tensile test. The final resistance for strain range 25%, 50%, and 75% is 165 Ω, 332 Ω, and 1.1 kΩ, respectively. Furthermore, upon release of the strain sensor, the sensor reverts back to its initial resistance without noticeable hysteresis. In addition to the tensile strain sensing, the $Ti_3C_2T_x$/PPy/PVDF sensor also demonstrate torsional motion. Figure 5e shows the relative resistance change during torsion deformation of the sensor. As the twist angle increase from 0, $\pi/2$, π, $3\pi/2$, and 2π radians, the corresponding resistance changes from 0 to 2 kΩ with a subsequent increment of 2 kΩ until the sensor is fully twisted at 360°. As the deformation is released, the resistance change recovers and returns to the initial state with a difference of 745 Ω. Figure 5f demonstrates that during 1000 s cyclic stability test, the sensor undergoes a stretching-releasing cycle and shows a stable resistance response with good reversibility due to the strong interfacial interaction of the conductive layer.

The developed $Ti_3C_2T_x$/PPy/PVDF film is demonstrated as a wearable strain sensor, whereby the real-time electrical signal response in monitoring different human body motions is shown in Figure 6. The output signal shows a clear resistance change when the wrist is bend as shown in Figure 6a. Stable signal response is observed as the bending cycle with a resistance change of 22% is repeated. Figure 6b shows knee bending, represented by the squat and rising. The ER of the sensor increased rapidly by 17%, and in subsequent repeated action, the sensor was able to detect and maintain resistance change to the initial level. Besides large stretch and bending motions, small stretch human body parts are investigated. Finger motion monitoring includes actions of finger bending and straightening. The stable waveform is observed in Figure 6c,d, where bending cycles are repeated with 50% and 100% resistance changes, respectively. The difference is due to the frequency of finger bending. Essentially, the output signals correspond with the movements in which the resistance change is repeated in a similar amplitude. As shown in Figure 6e,f, human joint motions are monitored and investigated. Both biceps and ankle stretching demonstrate reproducible stretching cycles. During the initial stretch, ER value increases rapidly and changes until the sensor recovers to its original state. The bending and recovery test results indicate the sensor has reliability and durability in the application for human motion monitoring. The proof-of-concept in this demonstration of the $Ti_3C_2T_x$/PPy/PVDF sensor suggests the potential of the fabricated sensor to be employed in the area of health care diagnostic and physical management.

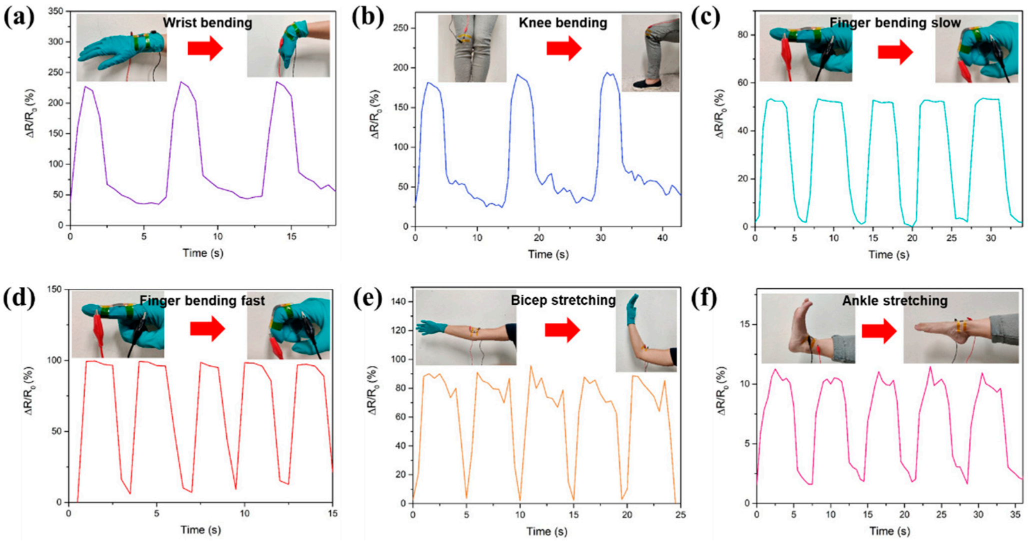

Figure 6. Application of the sensor in monitoring human body movement. (**a**) wrist bending (**b**) knee bending (**c**) finger bending at a slow pace (**d**) finger bending at a fast pace (**e**) bicep stretching (**f**) ankle stretching.

6. Conclusions

In summary, the $Ti_3C_2T_x$ based strain sensor is successfully fabricated with a strategic configuration of $Ti_3C_2T_x$ doped with Polypyrrole on flexible electrospun PVDF fiber. The fabricated composite of the substrate with microcracks exhibits a balance of sensitivity and sensing range that could be suitable for multiscale sensing. The hybrid structure of electrospun fiber as a foundation provides a percolation network for conductive filler network formation, which endows the sensor with excellent sensitivity. The fabricated sensor shows sensing performance characterized by sensitivity with a gauge factor of 78–355.32 with a sensing range of 0–100%. Besides its sensing properties, the sensor can be adopted for real-time human motion detection, thus providing a feasible approach for wearable strain sensors for healthcare monitoring.

Author Contributions: Conceptualization and project outline, M.R.A. and M.S.M.S.; perform experiments and measurements, W.X.R.L. and A.M.A.-D.; writing—original draft preparation, W.X.R.L.; writing—review and editing, M.S.M.S. All authors have read and agreed to the published version of the manuscript.

Funding: This research was funded by LRF-ICON, grant number 015ME0-048 and URIF, grant number 015LLB0-020.

Conflicts of Interest: The authors declare no conflict of interest.

References

1. Naguib, M.; Kurtoglu, M.; Presser, V.; Lu, J.; Niu, J.; Heon, M.; Hultman, L.; Gogotsi, Y.; Barsoum, M.W. Two-Dimensional Nanocrystals Produced by Exfoliation of Ti_3AlC_2. *Adv. Mater.* **2011**, *23*, 4248–4253. [CrossRef] [PubMed]
2. Naguib, M.; Mochalin, V.N.; Barsoum, M.W.; Gogotsi, Y. 25th Anniversary Article: MXenes: A New Family of Two-Dimensional Materials. *Adv. Mater.* **2014**, *26*, 992–1005. [CrossRef] [PubMed]
3. Hantanasirisakul, K.; Gogotsi, Y. Electronic and Optical Properties of 2D Transition Metal Carbides and Nitrides (MXenes). *Adv. Mater.* **2018**, *30*, 1804779. [CrossRef] [PubMed]
4. Li, X.; Wang, C.; Cao, Y.; Wang, G. Functional MXene Materials: Progress of Their Applications. *Chem. Asian J.* **2018**, *13*, 2742–2757. [CrossRef] [PubMed]
5. Ronchi, R.M.; Arantes, J.T.; Santos, S.F. Synthesis, Structure, Properties and Applications of MXenes: Current Status and Perspectives. *Ceram. Int.* **2019**, *45*, 18167–18188. [CrossRef]
6. Zhang, Y.-Z.; Lee, K.H.; Anjum, D.H.; Sougrat, R.; Jiang, Q.; Kim, H.; Alshareef, H.N. MXenes Stretch Hydrogel Sensor Performance to New Limits. *Sci. Adv.* **2018**, *4*, eaat0098. [CrossRef] [PubMed]
7. Ma, Y.; Liu, N.; Li, L.; Hu, X.; Zou, Z.; Wang, J.; Luo, S.; Gao, Y. A Highly Flexible and Sensitive Piezoresistive Sensor Based on MXene with Greatly Changed Interlayer Distances. *Nat. Commun.* **2017**, *8*, 1207. [CrossRef]

8. Ling, Z.; Ren, C.E.; Zhao, M.-Q.; Yang, J.; Giammarco, J.M.; Qiu, J.; Barsoum, M.W.; Gogotsi, Y. Flexible and Conductive MXene Films and Nanocomposites with High Capacitance. *Proc. Natl. Acad. Sci. USA* **2014**, *111*, 16676–16681. [CrossRef] [PubMed]
9. Liu, R.; Li, W. High-Thermal-Stability and High-Thermal-Conductivity Ti3C2Tx MXene/Poly(Vinyl Alcohol) (PVA) Composites. *ACS Omega* **2018**, *3*, 2609–2617. [CrossRef]
10. Sobolčiak, P.; Ali, A.; Hassan, M.K.; Helal, M.I.; Tanvir, A.; Popelka, A.; Al-Maadeed, M.A.; Krupa, I.; Mahmoud, K.A. 2D Ti3C2Tx (MXene)-Reinforced Polyvinyl Alcohol (PVA) Nanofibers with Enhanced Mechanical and Electrical Properties. *PLoS ONE* **2017**, *12*, e0183705. [CrossRef]
11. Naguib, M.; Saito, T.; Lai, S.; Rager, M.S.; Aytug, T.; Parans Paranthaman, M.; Zhao, M.-Q.; Gogotsi, Y. Ti3C2Tx (MXene)–Polyacrylamide Nanocomposite Films. *RSC Adv.* **2016**, *6*, 72069–72073. [CrossRef]
12. Zhang, H.; Wang, L.; Chen, Q.; Li, P.; Zhou, A.; Cao, X.; Hu, Q. Preparation, Mechanical and Anti-Friction Performance of MXene/Polymer Composites. *Mater. Des.* **2016**, *92*, 682–689. [CrossRef]
13. Zhi, W.; Xiang, S.; Bian, R.; Lin, R.; Wu, K.; Wang, T.; Cai, D. Study of MXene-Filled Polyurethane Nanocomposites Prepared via an Emulsion Method. *Compos. Sci. Technol.* **2018**, *168*, 404–411. [CrossRef]
14. Boota, M.; Pasini, M.; Galeotti, F.; Porzio, W.; Zhao, M.-Q.; Halim, J.; Gogotsi, Y. Interaction of Polar and Nonpolar Polyfluorenes with Layers of Two-Dimensional Titanium Carbide (MXene): Intercalation and Pseudocapacitance. *Chem. Mater.* **2017**, *29*, 2731–2738. [CrossRef]
15. Nezakati, T.; Seifalian, A.; Tan, A.; Seifalian, A.M. Conductive Polymers: Opportunities and Challenges in Biomedical Applications. *Chem. Rev.* **2018**, *118*, 6766–6843. [CrossRef]
16. Li, M.; Li, H.; Zhong, W.; Zhao, Q.; Wang, D. Stretchable Conductive Polypyrrole/Polyurethane (PPy/PU) Strain Sensor with Netlike Microcracks for Human Breath Detection. *ACS Appl. Mater. Interfaces* **2014**, *6*, 1313–1319. [CrossRef]
17. Bhatta, T.; Maharjan, P.; Cho, H.; Park, C.; Yoon, S.H.; Sharma, S.; Salauddin, M.; Rahman, M.T.; Rana, S.M.S.; Park, J.Y. High-Performance Triboelectric Nanogenerator Based on MXene Functionalized Polyvinylidene Fluoride Composite Nanofibers. *Nano Energy* **2021**, *81*, 105670. [CrossRef]
18. Alhabeb, M.; Maleski, K.; Anasori, B.; Lelyukh, P.; Clark, L.; Sin, S.; Gogotsi, Y. Guidelines for Synthesis and Processing of 2D Titanium Carbide (Ti_3C_2Tx MXene). *Chem. Mater.* **2017**, *29*, 7633–7644. [CrossRef]
19. Al-Dhahebi, A.M.; Ling, J.; Krishnan, S.G.; Yousefzadeh, M.; Elumalai, N.K.; Saheed, M.S.M.; Ramakrishna, S.; Jose, R. Electrospinning Research and Products: The Road and the Way Forward. *Appl. Phys. Rev.* **2022**, *9*, 011319. [CrossRef]
20. Xue, J.; Wu, T.; Dai, Y.; Xia, Y. Electrospinning and Electrospun Nanofibers: Methods, Materials, and Applications. *Chem. Rev.* **2019**, *119*, 5298–5415. [CrossRef]
21. Al-Dhahebi, A.M.; Gopinath, S.C.B.; Saheed, M.S.M. Graphene Impregnated Electrospun Nanofiber Sensing Materials: A Comprehensive Overview on Bridging Laboratory Set-up to Industry. *Nano Converg.* **2020**, *7*, 1–23. [CrossRef] [PubMed]
22. Al-Dhahebi, A.M.; Jose, R.; Mustapha, M.; Saheed, M.S.M. Ultrasensitive Aptasensor Using Electrospun MXene/Polyvinylidene Fluoride Nanofiber Composite for Ochratoxin A Detection. *Food Chem.* **2022**, *390*, 133105. [CrossRef] [PubMed]
23. Al-Dhahebi, A.M.; Saheed, M.S.M.; Mustapha, M. Effects of Solution Concentration on the Synthesis of Polyvinylidene Fluoride (PVDF) Electrospun Nanofibers. *Mater. Today Proc.* **2021**. [CrossRef]
24. Lin, C.; Luo, S.; Meng, F.; Xu, B.; Long, T.; Zhao, Y.; Hu, H.; Zheng, L.; Liao, K.; Liu, J. MXene/Air-Laid Paper Composite Sensors for Both Tensile and Torsional Deformations Detection. *Compos. Commun.* **2021**, *25*, 100768. [CrossRef]
25. Zheng, J.; He, A.; Li, J.; Han, C.C. Polymorphism Control of Poly(Vinylidene Fluoride) through Electrospinning. *Macromol. Rapid Commun.* **2007**, *28*, 2159–2162. [CrossRef]
26. Zheng, Y.; Jin, Q.; Chen, W.; Sun, Y.; Wang, Z. High Sensitivity and Wide Sensing Range of Stretchable Sensors with Conductive Microsphere Array Structures. *J. Mater. Chem. C* **2019**, *7*, 8423–8431. [CrossRef]
27. Xu, M.; Li, X.; Jin, C.; He, Z.; Zhang, Q. High-Performance Epidermal Strain Sensor Based on Macro-Defect Graphene Foams. *Sens. Actuators A Phys.* **2020**, *303*, 111721. [CrossRef]
28. Yue, X.; Jia, Y.; Wang, X.; Zhou, K.; Zhai, W.; Zheng, G.; Dai, K.; Mi, L.; Liu, C.; Shen, C. Highly Stretchable and Durable Fiber-Shaped Strain Sensor with Porous Core-Sheath Structure for Human Motion Monitoring. *Compos. Sci. Technol.* **2020**, *189*, 108038. [CrossRef]
29. Zhou, S.; Gu, C.; Li, Z.; Yang, L.; He, L.; Wang, M.; Huang, X.; Zhou, N.; Zhang, Z. Ti3C2Tx MXene and Polyoxometalate Nanohybrid Embedded with Polypyrrole: Ultra-Sensitive Platform for the Detection of Osteopontin. *Appl. Surf. Sci.* **2019**, *498*, 143889. [CrossRef]
30. Rajavel, K.; Luo, S.; Wan, Y.; Yu, X.; Hu, Y.; Zhu, P.; Sun, R.; Wong, C. 2D $Ti_3C_2T_x$ MXene/Polyvinylidene Fluoride (PVDF) Nanocomposites for Attenuation of Electromagnetic Radiation with Excellent Heat Dissipation. *Compos. Part A Appl. Sci. Manuf.* **2020**, *129*, 105693. [CrossRef]
31. Barlian, A.A.; Park, W.-T.; Mallon, J.R.; Rastegar, A.J.; Pruitt, B.L. Review: Semiconductor Piezoresistance for Microsystems. *Proc. IEEE* **2009**, *97*, 513–552. [CrossRef] [PubMed]
32. Zhao, L.; Wang, K.; Wei, W.; Wang, L.; Han, W. High-Performance Flexible Sensing Devices Based on Polyaniline/MXene Nanocomposites. *InfoMat* **2019**, *1*, 407–416. [CrossRef]
33. Pan, J.; Yang, M.; Luo, L.; Xu, A.; Tang, B.; Cheng, D.; Cai, G.; Wang, X. Stretchable and Highly Sensitive Braided Composite Yarn@Polydopamine@Polypyrrole for Wearable Applications. *ACS Appl. Mater. Interfaces* **2019**, *11*, 7338–7348. [CrossRef] [PubMed]

34. Yao, S.; Zhu, Y. Wearable Multifunctional Sensors Using Printed Stretchable Conductors Made of Silver Nanowires. *Nanoscale* **2014**, *6*, 2345–2352. [CrossRef] [PubMed]
35. Fu, X.-W.; Liao, Z.-M.; Zhou, J.-X.; Zhou, Y.-B.; Wu, H.-C.; Zhang, R.; Jing, G.; Xu, J.; Wu, X.; Guo, W.; et al. Strain Dependent Resistance in Chemical Vapor Deposition Grown Graphene. *Appl. Phys. Lett.* **2011**, *99*, 213107. [CrossRef]
36. Chang, X.; Sun, S.; Sun, S.; Liu, T.; Xiong, X.; Lei, Y.; Dong, L.; Yin, Y. ZnO Nanorods/Carbon Black-Based Flexible Strain Sensor for Detecting Human Motions. *J. Alloys Compd.* **2018**, *738*, 111–117. [CrossRef]